Improved Single Ended Traveling Wave Fault Location Algorithm Based On Experience With Conventional Substation Transducers

D. J. Spoor, and J. Zhu, Senior Member, IEEE

***Abstract*-- Single-ended unsynchronized traveling wave fault location algorithms have been around for several years. They avoid the costs and complexities associated with remote end synchronization. Nevertheless, there is a corresponding increase in required signal processing as each reflection must be identified and then related in time to the signal wave front.**

The current signal processing techniques include a combination of modal and wavelet analysis, where the resulting vectors are often squared. However, the performance of this process degrades dramatically with the filtering associated with the substation transducers and secondary circuits. Furthermore, the variation in observed reflection patterns demonstrates that these methods cannot adequately distinguish between faults on the near, or far half of the transmission line.

This paper considers the traveling wave data observed on a 330kV transmission system and presents a new signal processing methodology to cater for the observations. This is based on the continuous wavelet transform that is calculated at a suitably large scale. The polarities of the resulting coefficients are used to confirm the nature of the fault, and to infer the true fault location.

***Index Terms*-- Current transformers, Fault location, Traveling wave devices, Transmission lines, Wavelet transforms**

I. Introduction

The use of fault location systems on transmission circuits can aid by improving the system availability and performance, as well as reducing the operating costs and losses in deregulated electricity markets.

Traveling wave fault location techniques are recognized as some of the most accurate methods currently in use. Several types have been documented in [1] although these can generally be categorized as synchronized or unsynchronized.

The synchronized algorithm is the most predominant on overhead transmission lines, and calculates the fault location based on the relative arrival times of the traveling wave transients at each terminal using a synchronizing clock.

Unsynchronized algorithms identify the location of the fault by observing the time delay between successive reflections in the traveling wave signal observed at one location. This is similar to the off-line approach of time domain reflectometry, which has been used very successfully on de-energized cables and transmission lines with the aid of accurate transducers.

These single-ended traveling wave algorithms avoid the costs and complexities associated with remote end synchronization. Nevertheless, there is a corresponding increase in the required signal processing as each reflection must be identified and then related in time to the signal wave front.

Such algorithms have been noted as being too complex and erroneous for operations personnel to accurately locate faults [2], due to the problems with distinguishing between traveling waves reflected from the fault and from the remote end of the line [3]. In some situations, it may also be difficult to identify the true wave front of the recorded signal as the transient can become lost in the disturbances created by a previous event.

As a result, many implementations incorporate other technologies. For instance, the single ended, unsynchronized algorithm has been combined with a one-terminal impedance based fault location algorithm [4,5]. However, many other single ended implementations still require the operator to manually identify the forefront of the initial transient.

The approaches adopted in [6] and [7] are indicative of the signal processing methods that have recently been proposed. Here, the traveling wave transients are decoupled into their modal components, and are then further decomposed into their wavelet coefficients using the discrete wavelet transform (DWT). This gives simulated accuracies better than 3 miles on a 200 mile circuit.

Abur [3] has also proposed an algorithm for single ended fault location that distinguishes between grounded and ungrounded faults from the ground mode signals. These are applied to a threshold on the DWT^2 vector. If the fault is grounded, and the wavelet transform of the ground mode signal is small, the fault is in the remote half of the line, and vice versa.

The techniques presented in [3] and [8] also conclude that the traveling wave signals can be adequately identified using discrete wavelet analysis with a scale of 1, where the resulting coefficients are squared (DWT^2).

However, the combined effect of the sampling rate, the poor frequency response of many substation transducers, and the variation in reflection patterns appear to give erroneous results when applying these techniques to observed data. This paper presents an alternate wavelet approach that provides a reliable fault location estimate under these conditions.

D. J. Spoor was with Transgrid, Sydney, New South Wales, Australia during the development of this paper. He is now with Integral Energy, Sydney, New South Wales, Australia (e-mail: darren.spoor@integral.com.au).

J. Zhu is with the Department of Electrical Engineering, University of Technology, Sydney, Australia (e-mail: joe@eng.uts.edu.au).

II. Signal Processing Techniques

This section describes the common traveling wave signal processing methods required for three-phase lines. A good overview of the Fourier, windowed Fourier and wavelet transforms is provided in [8,9]. However, several authors have recognized the benefits of applying modal analysis in conjunction with the wavelet transform. Reference [3] specifically presents the discrete wavelet transform as one of the best for identifying traveling wave transients on power systems.

A. Modal Analysis

Using a modal transformation, the phase signals can be decoupled into several independent modes of propagation. For a three-phase system, the transformed quantities will contain one ground mode and two independent aerial modes, which travel close to the speed of light on overhead circuits. Conversely, the earth mode signals travel at a somewhat slower velocity with a higher attenuation. This earth mode, as with the transmission line zero sequence impedance, is frequency dependant due to the non-uniform distribution of the earth current. On the other hand, the aerial modes can be assumed to be frequency independent.

Clarke's matrix is one of several commonly used transformation matrices: [10]

$$\begin{bmatrix} I^{(0)}(t) \\ I^{(1)}(t) \\ I^{(2)}(t) \end{bmatrix} = \frac{1}{3}\begin{bmatrix} 1 & 1 & 1 \\ 2 & -1 & -1 \\ 0 & \sqrt{3} & -\sqrt{3} \end{bmatrix}\begin{bmatrix} I_A(t) \\ I_B(t) \\ I_C(t) \end{bmatrix} \quad (1)$$

where I_A, I_B and I_C are the phase currents, I_0, is the ground mode current and I_1 and I_2 are the decoupled aerial modes.

Such simple transformations are real and assume a transposed circuit. Untransposed circuits require an eigenvalue based transformation matrix that is frequency dependent [11]. However, most untransposed lines may be assumed as transposed for the purposes of identifying the modal parameters.

B. Continuous Wavelet Transform

Wavelet techniques maintain the correlation between time and frequency for the observed signal. This proves to be advantageous in determining the wave front of the traveling wave and the subsequent reflections.

The continuous wavelet transform (CWT) is defined as the sum over time of the input signal *f(t)* multiplied by scaled, shifted versions of the wavelet function Ψ:

$$CWT(a,b) = \frac{1}{\sqrt{|a|}}\int_{-\infty}^{\infty} f(t)\psi^*\left(\frac{t-b}{a}\right)dt \quad (2)$$

The coefficients *a* and *b* are the scaling and translation constants respectively. These can be used to alter the characteristics of the 'mother' wavelet function, which may be either real or complex [8,3]. The wavelet function itself can be of any particular form as long as it complies with the admissibility conditions presented in [10].

Using a continuous scale of *a* and *b* results in many wavelet coefficients, some of which are redundant due to the similarity to those produced at other close scales. The pseudo-frequency which corresponds to each coefficient is proportional to the scale factor *a*, the sampling period T_S of the input signal, and the centre frequency for the particular wavelet function F_C, as the following: [12]

$$frequency = T_S F_C / a \quad (3)$$

The first (and lowest) scales have the highest time resolution, and cover a broad frequency range at the high end of the spectrum. The frequency resolutions of these scales are only limited by the sampling rate of the input signal. Conversely, higher scales cover an increasingly longer time interval and correspond to the lower end of the frequency spectrum.

C. Discrete Wavelet Transform

The Discrete Wavelet Transform overcomes some of the problems associated with obtaining redundant coefficients. The DWT algorithm is not continuously scaleable and translatable. Instead it can only be adjusted in discrete steps, resulting in a piecewise continuous function:

$$DWT(m,n) = \frac{1}{\sqrt{a_0^m}}\sum_k f(k)\psi^*\left(\frac{n - ka_0^m}{a_0^m}\right) \quad (4)$$

Here, the scaling and translation parameters are replaced with a_0^m and ka_0^m, where *k* and *m* are integers, and $a_0>1$ is the fixed dilation step. The DWT determines the coefficients on a dyadic basis rather than a continuous shifting and scaling as with the CWT.

When implementing the DWT, the signal *f(k)* is applied to a multi-stage filter bank [9] where $a_0=2$ and *m* is the level of decomposition. Downsampling is performed at the output of each low-pass filter within the filter bank in preparation for the next stage. Consequently, the scale has an inverse relationship to the frequency [10], and the resulting series of wavelet coefficients is referred to as the wavelet series decomposition [8]. The pseudo-frequency corresponding to a particular level of decomposition *m*, or scale a_0^m can be determined from:

$$frequency = T_S F_C / a_0^{\,m} \quad (5)$$

In principle, any admissible wavelet can be used in wavelet analysis [12]. Similar to the observations made in [13], the differences between the results obtained from many well-known wavelets in the following analysis were small, and so the sym2 wavelet has been used in all cases.

III. Transducer Selection and Frequency Response

On-line traveling wave fault location techniques require transducers capable of withstanding power system voltages. High voltage transducers with a large dynamic range are available for these applications, such as optical current

transducers and Rogowski-Chattock coils. However, the additional installation costs and the requirement to take high voltage equipment out of service during installation is often a major limitation in their use. The overall commissioning costs are a significant factor, as traveling wave techniques must compete with cheaper impedance-based algorithms incorporated in most protection relays and fault recorders.

As a result, conventional substation transducers are often the only economic means of monitoring the voltage or current transients during normal operation. In most cases this means that the traveling wave recorder is connected via split-core inductive couplers to the secondary protection circuits from the substation current transformers. Unfortunately, this approach can constrain the accuracy in the fault location due to the band-pass nature of the secondary circuit [14].

The transfer function response of the substation current transformer and secondary cabling can be calculated using the approach presented in [15].

The analysis considered in this paper is based on the observations from a particular 330kV double circuit line, 186km in length and with traveling wave recorders permanently installed at each end. A similar system was described in [2,16,17]. These recorders sample the line currents at 1.25MHz with an 8-bit resolution via inductive couplers on the substation protection secondary circuits. The traveling wave systems are designed to use a synchronized algorithm, and so have a common GPS time base with a 1μs resolution [13]. GPS is a worldwide satellite system incorporating 24 satellites which orbit the earth twice a day. Each of the GPS receivers provide 1PPS (pulse per second) signal synchronized 1MHz clock.

Fig.1 shows the correlation between scale and pseudo-frequency for the 'sym2' wavelet function where the sampling rate is 1.25MHz. Similarly, the frequency response of the aerial mode currents in this installation is shown in Fig. 2, where the current in the substation secondary circuit is calculated relative to the primary line current for a traveling wave installation on Transgrid's 330kV network. The response is highly dependant on the length and type of secondary cabling, the current transformer parameters and the resistance and inductance of the relay burden. Noting that the traveling wave recorder samples at 1.25MHz, the current transformer and secondary circuit clearly impacts the higher frequency components and the corresponding smaller wavelet scales.

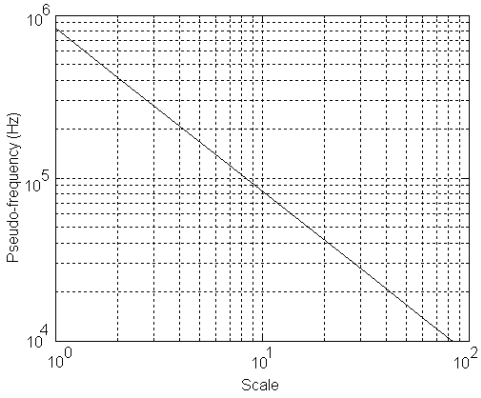

Fig. 1. Calculated pseudo-frequency at various scales for the sym2 wavelet with a sampling rate of 1.25MHz

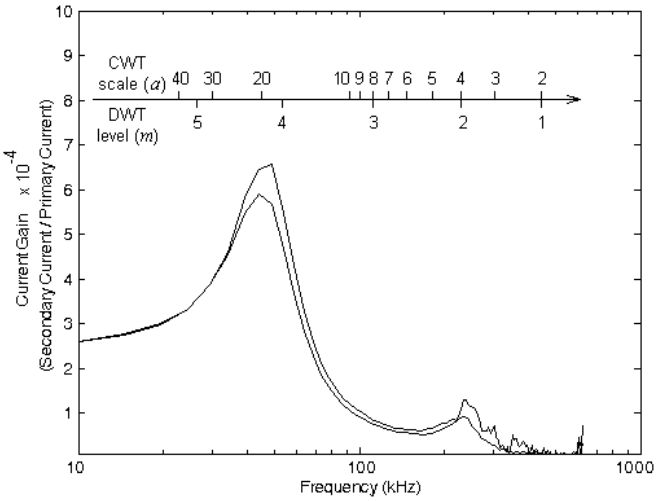

Fig. 2. Frequency response of current transformer, secondary cabling and relay burden compared to various CWT scales and DWT levels

IV. The Unsynchronized Traveling Wave Algorithm

Single ended traveling wave algorithms have primarily been implemented by recording the time difference between successive reflections observed at one end of the line. Here, ΔT is the time between these reflections, and T_L is the line reflection travel time

$$m = \Delta T \times \frac{v}{2} \tag{6}$$

$$T_L = \frac{2l}{v} \tag{7}$$

where, l is the line length and v is the average velocity of the aerial modes.

This technique has shown a high level of accuracy in simulation. However several limitations exist when applied to the data obtained from conventional transducers.

A. Discrete and Continuous Wavelet Applications

Single ended wavelet calculations performed on observed data indicate that the performance of the DWT technique degrades dramatically due to the filtering associated with the substation transducers and secondary cabling.

The coupling between the modes in the secondary cabling of the substation current transformers can result in 'apparent' ground mode oscillations, whether the fault was grounded or not. Similarly, the resonant nature of the secondary cabling can produce several decaying peaks in the DWT[2] vector where only one reflection previously existed. Moreover, the DWT has poor noise rejection when applied to digitized data with significant quantization errors.

Figs. 3 to 6 compare the DWT and CWT techniques for an observed fault, 71.6km from the recorder. This is compared to a simulation of an identical fault on this particular circuit using the Alternative Transients Program (ATP) where a simulation frequency of 1.25MHz was also used and ideal coupling transducers have been assumed.

As shown in Figs. 3 and 5, Both the DWT and CWT

algorithms appear to have a high degree of accuracy when applied to simulated data. However, the observed traveling wave signals are less recognizable in the scale 1 and scale 2 DWT vectors due to the filtering imposed by the secondary cabling.

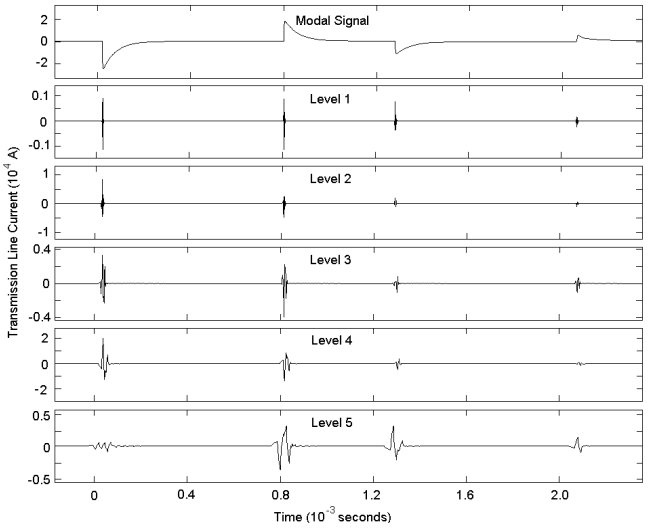

Fig. 3. DWT coefficients for a simulated incipient fault at 71.6km

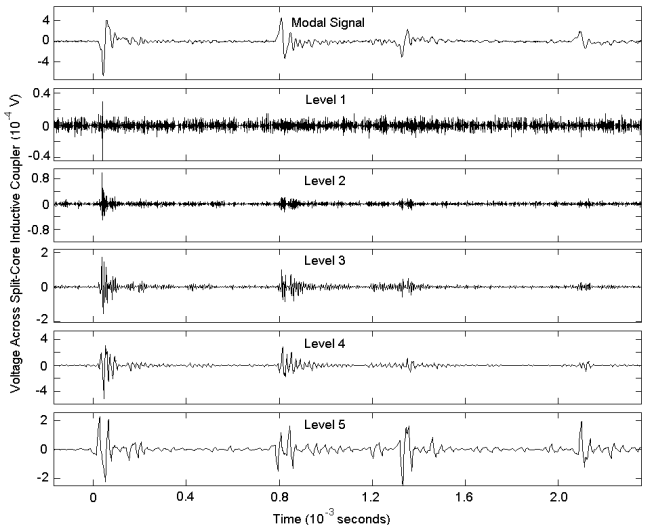

Fig. 4. DWT coefficients for an observed incipient fault at 71.6km

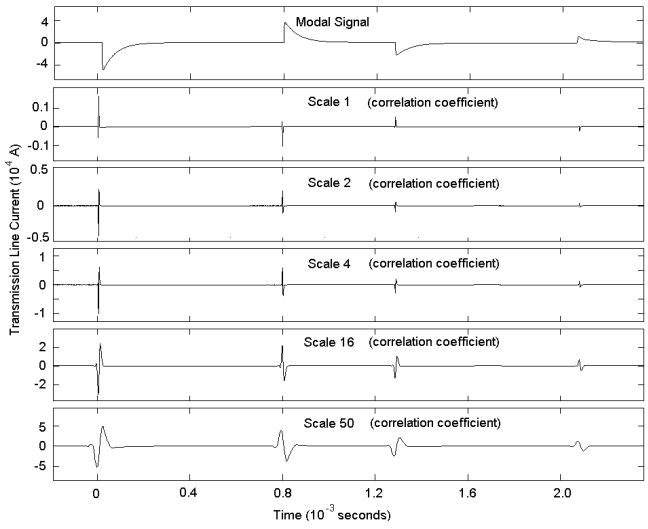

Fig. 5. CWT coefficients for the simulated incipient fault at 71.6km

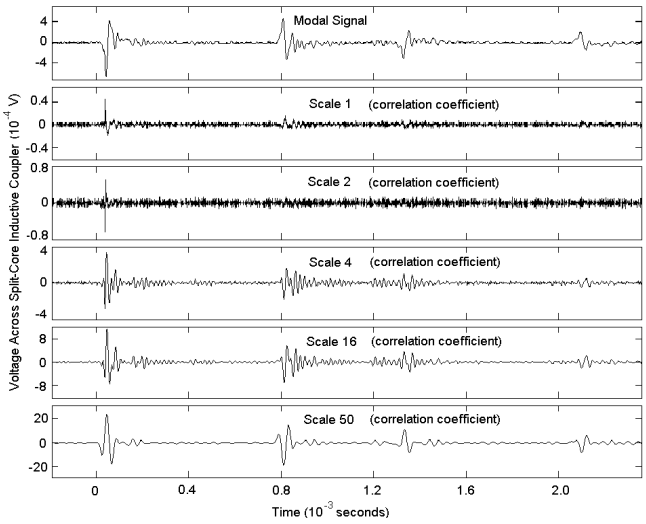

Fig. 6. CWT coefficients for the observed incipient fault at 71.6km

A similar loss of resolution at high frequencies is seen in the CWT calculations, although the CWT technique appears to maintain a good resolution when using a large scale for the correlation. Consequently, it appears that the DWT cannot be adequately applied to a noisy, filtered signal, as is commonly observed using conventional substation current transformers.

B. Solid and Incipient Faults

One of the difficulties with single ended techniques is in distinguishing between faults on the near and remote half of the transmission line. This is particularly relevant for high impedance faults that can create reflection patterns similar to both a solid and incipient fault.

Incipient faults are discharges that are short in duration, resulting in few (if any) reflections from the fault itself, whereas solid faults are characterized by long fault durations and strong repetitive reflections from the fault.

Since the CWT algorithm appears to provide a consistent and reliable analysis of observed traveling wave transients at a large scale, the CWT^2 vectors for simulated incipient and solid faults have been shown in Figs. 7 and 8. Each simulation incorporated a fault that was located at 30% of the line length from the monitored busbar. It is clear that the conventional unsynchronised traveling wave algorithm will give an erroneous location estimate for the incipient fault.

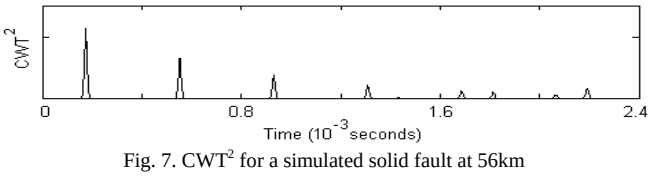

Fig. 7. CWT^2 for a simulated solid fault at 56km

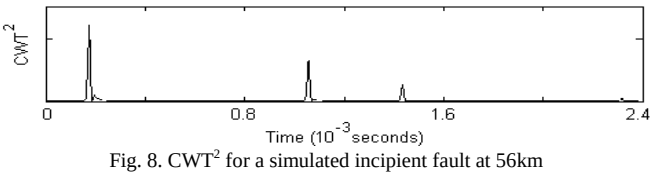

Fig. 8. CWT^2 for a simulated incipient fault at 56km

However, the polarity of the CWT pulse is a valuable key to identifying the nature of the fault, and consequently the fault location. As a result, the $CWT^{|2|}$ is proposed to distinguish between solid and incipient faults by considering the polarity of the reflections that occur within the line travel time T_L.

$$CWT^{|2|} = CWT \times |CWT| \tag{8}$$

Due to the transient reflection coefficient at the busbars and the fault itself, solid faults characteristically produce 'pulses' of the same polarity within the $CWT^{|2|}$ decomposition, which are equally spaced from the initial wave front. However, the incipient fault has opposing polarities and no symmetry within the time T_L.

Figs. 9 and 10 show the $CWT^{|2|}$ vectors for a simulated solid and incipient fault at 56km. The fault currents were obtained from an ATP simulation of the 330kV double circuit line, sampled at 1.25MHz. Following a modal decomposition, the aerial mode with the greatest magnitude was used to calculate the $CWT^{|2|}$ at a scale of 45. In the following diagrams, T_L corresponds to approximately 1.3ms.

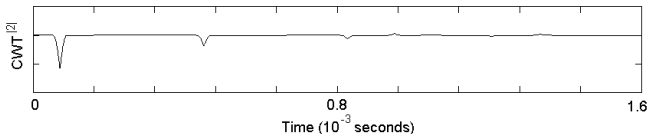

Fig. 9. $CWT^{|2|}$ for a simulated solid fault at 56km

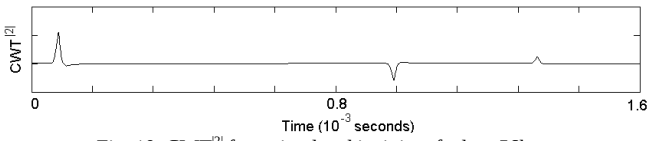

Fig. 10. $CWT^{|2|}$ for a simulated incipient fault at 56km

Similarly, Figs. 11 and 12 illustrate the $CWT^{|2|}$ vector obtained from the observed waveforms, where the solid fault was identified at 49km and the incipient fault was located 72km from the recording device. In this scenario, a conventional unsynchronized algorithm using the DWT^2 or CWT^2 vector would give an erroneous fault location for the incipient fault.

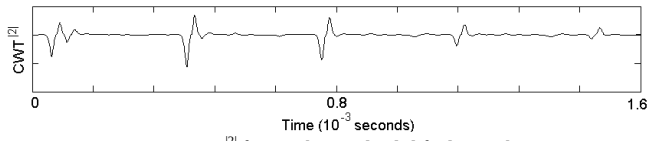

Fig. 11. $CWT^{|2|}$ for an observed solid fault at 49km

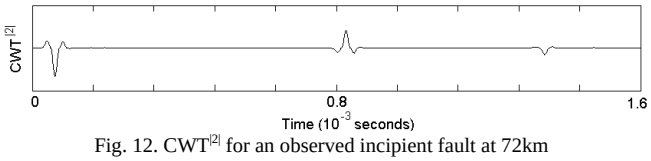

Fig. 12. $CWT^{|2|}$ for an observed incipient fault at 72km

C. The proposed algorithm

To accurately determine the fault location from a recorded single ended transient, a scale should be selected based on the filtering characteristics of the coupling transducer. According to the transducers and sampling frequency used in this paper, a scale of at least 20 should be chosen.

The CWT coefficient vector is then calculated from the predominant aerial mode using this scaling factor. From this same aerial mode, the CWT^2 and the $CWT^{|2|}$ coefficient vectors are calculated at the selected scale.

The initial transient and the first reflection are identified from a threshold applied to the CWT^2 vector. However, the polarity of the first reflection should be compared to the initial wavefront based on the coefficients in the $CWT^{|2|}$ vector.

Should the polarity of each transient differ, the location m can be calculated from:

$$m = l - \Delta T \times \frac{v}{2} \tag{8}$$

Alternatively, the same polarity indicates that the reflection has occurred as a result of a solid fault. In this case, the fault location can be determined from:

$$m = \Delta T \times \frac{v}{2} \tag{9}$$

D. High Impedance Faults

High impedance faults are often caused by contact with vegetation and occur frequently on transmission and distribution systems. The reflection patterns observed from such faults have characteristics that are common to both an incipient and a solid fault. This creates a difficulty in identifying the location for faults symmetrically applied around 50% of the line length.

Fig. 13 shows the $CWT^{|2|}$ vector observed for a high impedance fault observed in 2001, where the fault was located approximately 64km from the monitored busbar, and a scale of 45 was adopted. The transient identified by *A* corresponds to the initial wavefront of the traveling wave; *B* is the reflection of the initial pulse *A* off the fault itself; *C* is the initial reflection from the remote busbar, and *D* is the first reflection of the initial transient *A* from the remote busbar. Transient *D* also corresponds to the line travel time T_L.

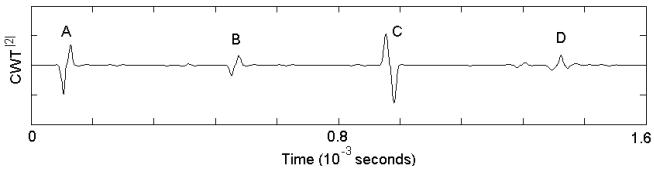

Fig. 13. High impedance fault located 63.6km from the monitored busbar

The impedance of this fault leads to transient *C* having a greater magnitude than *B*. Consequently, a location of 126.4km would be obtained if point *C* were chosen as the predominant reflection. However, the correct location of 63.6km is only calculated when using reflection *B*.

The polarity of the $CWT^{|2|}$ vector clearly shows the solid component reflected from the fault and the incipient component reflected from the busbar. This provides additional confirmation that the correct reflection has been selected for the calculation.

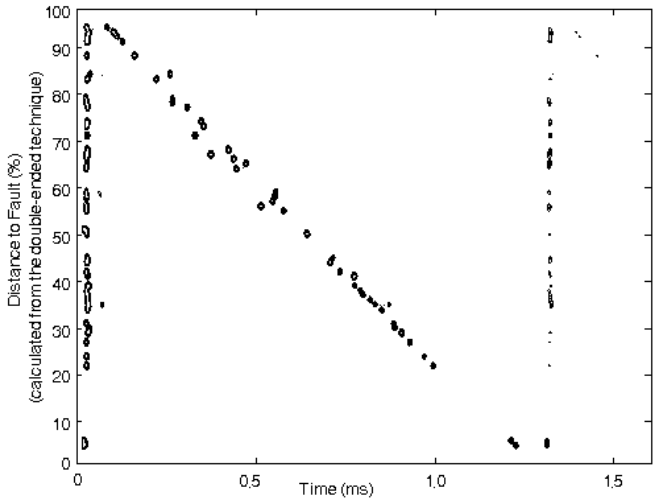

Fig. 14. CWT$^{|2|}$ contour peaks for several observed incipient faults

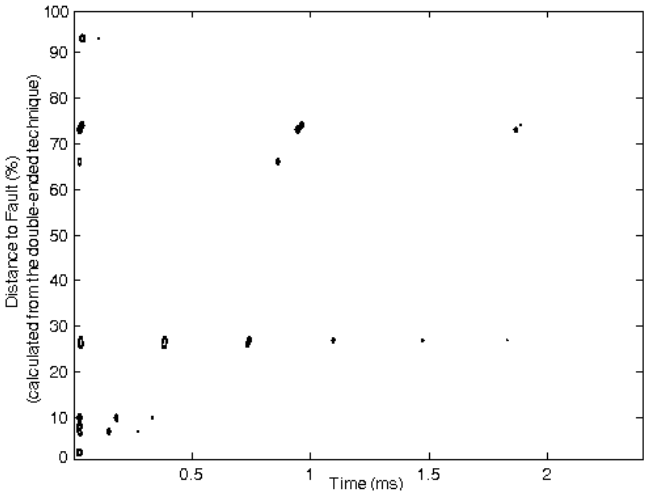

Fig. 15. CWT$^{|2|}$ contour peaks for several observed solid faults

E. Accuracy of the Single Ended Algorithm

To assess the accuracy of the proposed single ended traveling wave algorithm, the travel time T_L was measured from the CWT$^{|2|}$ vectors of 39 incipient faults since 1999. The resultant standard deviation in traveling times is approximately 1.2μs, which corresponds to 340m at the propagation velocity of the aerial mode.

Fig. 14 plots the peaks in the CWT$^{|2|}$ vectors in a contour form for each of the faults considered above. Note that the position of each fault on the vertical axis is based on the GPS synchronized calculations applicable for each fault. In this case, the fault location is determined from the relative arrival time of the transient at each end of the circuit, as the following:

$$m = \frac{l}{2} + \Delta T\left(\frac{v}{2}\right) \qquad (10)$$

where ΔT is the difference in observed signal times, v the aerial mode velocity of the circuit, and l the line length.

Consequently, the unsynchronized algorithm has the potential of increased resolution over the synchronized technique. This can be observed when the reflection patterns are visually compared with the synchronized fault location. The second or the diagonal portion of the scatter plot appears to vary considerably compared to the reflection from the remote busbar T_L. This variation corresponds to the added uncertainty imposed by the GPS and hardware timing errors in the synchronized traveling wave algorithm [18].

It is interesting to note that the first 20% of this line is constructed in a developed environment while the remainder of the circuit is primarily situated in relatively inaccessible terrain. This may partly explain why fewer incipient faults have been observed on this section of the transmission line.

Fig. 15 also shows the CWT$^{|2|}$ vectors for the solid faults observed on this particular circuit since 1999. Due to the limited number of faults, no additional comments on the observed accuracy have been made at this stage. Nevertheless, it is again interesting to note the contrasting reflection patterns between the observed solid and incipient faults on this particular circuit.

V. Conclusions

Commercial traveling wave systems usually employ conventional substation current transformers due to the expense and outage requirements associated with optical current transformers or Rogowski-Chattock coils.

Consequently, the performance of unsynchronized traveling wave fault location algorithms can be restricted by the frequency response of these non-ideal substation transducers. The resonant nature of the secondary cabling, current transformer and relay burden results in a significant observed filtering delay.

A comparison between the discrete and continuous wavelet algorithms on observed data demonstrates that the discrete wavelet transform can not be adequately applied to a noisy, or heavily filtered signal. As a result, the continuous wavelet transform is presented as the ideal approach to identifying signal reflections.

Unsynchronized fault location algorithms can further suffer from discrepancies between solid and incipient faults. However, clarification can be provided from the signal polarity of the continuous wavelet transform.

This paper has presented a simple and reliable approach to assist with the fault location calculation. This is based on the continuous wavelet transform, at a suitably large scale. The polarity of the resulting coefficients has then been used to confirm the nature of the fault, and the true fault location.

VI. References

[1] M. K. Hoi, "Travelling wave fault locator experience on CLP power transmission network," presented at the CEPSI conference, Fukuoka, 2002. *Paper T2-B-8*

[2] P. Gale and R. Burnett, "A study of power line response to lightning using GPS based travelling wave fault locators and the US national lightning detection network," Fault and Disturbance Analysis and Precise Measurements in Power Systems Conference, Arlington, Virginia, 1996.

[3] A. Abur and F. Magnago, "Fault location using wavelets," *IEEE Trans. Power Delivery*, vol. 13, pp. 1475-1480, Oct. 1988.

[4] V. Pathirana, P. McLaren, and E. Dirks, "Investigation of a hybrid travelling wave/impedance relay principle," *Proc. of IEEE Power Eng. Society Transmission and Distribution Conf., May 2002,vol.1*, pp. 48-53

[5] X. Dong, Z. Chen, X. He, K. Wang, and C. Luo, "Optimizing solution of fault location," *Proc. IEEE Power Eng. Society Summer Meeting, July 2002*, vol.3, pp. 1113-1117

[6] F. Magnago, and A. Abur, "A new fault location technique for radial distribution systems based on high frequency signals," *Proc. IEEE Power Eng. Soc. Trans. and Distribution Conf., July 1999,* vol.1, pp. 426-431

[7] X. Z. Dong, M. A. Redfern, Z. Bo, F. Jiang, "The application of the wavelet transform of travelling wave phenomena for transient based protection," Int. Conf. on Power Systems Transients, New Orleans, 2003

[8] P. Imris and M. Lehtonen, "A comparison of different signal processing techniques for travelling wave fault location," The 44th Int. Sci. Conf. of Riga Technical University, Riga, Latvia, 9-11 Oct. 2003, pp. 220-226.

[9] D. Robertson, O. Camps, J. Mayer and W. Gish, "Wavelets and electromagnetic power system transients," *IEEE Trans. Power Delivery*, vol. 11, Apr. 1996, pp. 1050-1058

[10] C. Valens. (1999). A really friendly guide to wavelets. [Online]. Available: http://mathforum.org/library/view/16425.html

[11] F. Brandao, B. Hildemaro "On the modal analysis of asymmetrical three-phase transmission lines using standard transformation matrices," *IEEE Trans. Power Delivery*, vol. 12, Oct. 1997, pp. 1760–1765

[12] M. Misti, Y. Misti, G. Oppenheim, J. Poggi, "Wavelet Toolbox User's Guide – Version 2", The Math Works Inc., Natick, MA

[13] G. Kim, H. Kim, J. Choi, "Wavelet transform based power transmission line fault location using GPS for accurate time synchronization," *Proc. IEEE Power Eng. Soc. Trans. and Distribution Conf., 2001,* vol1, pp. 495–499

[14] D. Spoor, J. Zhu, "Transfer function analysis of coupling equipment used for traveling wave fault location," *Proc. of* Int. Conf. on Electrical Machines and Systems, Jeju Island, Korea, Nov. 2004

[15] D. Spoor, J. Zhu, P. Nichols "Filtering effects of substation secondary circuits on power system traveling wave transients," *Proc.* Int. Conf. on Electrical Machines and Systems, Nanjing, China, Sept. 2005

[16] D.W.P. Thomas, C. Christopoulos, Y. Tang, T. Mustafa, A. Raizer:, "Measurement of high frequency propagation and coupling from recorded transients in EHV substations," School of Electrical and Electronic Engineering, The University of Nottingham, Nottingham NG7 2RD, UK

[17] T.I.A.H. Mustafa, D.W.P Thomas, C. Christopoulos, A. Raizer, "Comparison of simulated and recorded transients for travelling wave fault location," *IEEE Power Tech Conf. Proc.*, Bologna, June 2003, vol. 3

[18] A. Mink, R.J. Carpenter, M. Courson, "Time synchronised measurements in cluster computing systems," *Proc. IEEE Int. Conf. on Parallel and Distributed Computing*, Aug 2000, vol. 1, pp. 48-53

[19] Leuven EMTP Center, "Alternative Transients Program Rule Book," 1987

VII. BIOGRAPHIES

Darren Spoor was born in Sydney, Australia, in 1978. He received the undergraduate B.E. in electrical engineering degree in 2002, while he was with Transgrid, Sydney. He is currently pursuing the Ph.D. degree at the University of Technology, Sydney (UTS). focusing on protection and fault location for overhead transmission circuits.

Jian Guo Zhu (SM'03) received his B.E and M.E. degrees in China from Jiansu Institute of Technology in 1982 and Shanghai University of Technology in 1987, respectively, and the PhD degree from University of Technology, Sydney (UTS), Australia, in 1995. Currently, he is the Professor of Electrical Engineering at UTS. His research interests are electromagnetics and electrical machines and drives.